12th IFAC International Symposium on
Advanced Control of Chemical Processes
July 14-17, 2024. Toronto, Canada

An Unsupervised Machine Learning Approach for Process Monitoring by Visual Analytics

Hugo O. Garcés * **Bastián Aballay** *
Harikrishna Rao Mohan Rao ** **Tongwen Chen** **
Sirish L. Shah ***

* *Departamento Ingeniería Informática y Ciencias de la Computación, Universidad de Concepción, Concepción, Chile (e-mail: hugarces@inf.udec.cl, baballay@inf.udec.cl).*
** *Department of Electrical & Computer Engineering, University of Alberta, Edmonton, Alberta T6G 1H9, Canada. (e-mail: {mohanrao, tchen}@ualberta.ca).*
*** *Department of Chemical & Materials Engineering, University of Alberta, Edmonton, Alberta T6G 1H9, Canada. (e-mail: sirish.shah@ualberta.ca).*

Abstract: This paper examines the suitability of unsupervised machine learning methods for image analysis, within the innovative visual analytics framework for process monitoring, and proposes a set of performance metrics that evaluate accuracy for visual analytics. The effectiveness of the proposed method is demonstrated via a case study using real industrial data from a steam boiler.

Keywords: Process Monitoring, Signal Processing, Image Analysis, Fault Detection, Industrial Applications

1. INTRODUCTION

Systems & Control (S&C) challenges offer numerous opportunities for multidisciplinary research and development, driven by technologies such as Artificial Intelligence (AI), including machine learning and Big-Data (Annaswamy et al., 2023; Daoutidis et al., 2024). Recent studies highlight the potential of machine learning methods in providing S&C data-driven solutions through hybrid modeling, integrating mathematical programming or reinforcement learning, for tasks such as monitoring, control, and estimation of critical variables (Lawrence et al., 2024). At the core of data-driven solutions is the massive amount of sensor data from the process, which is increasingly available due to improved instrumentation technologies. However, the mere availability of sensor data does not guarantee improved process knowledge or optimal performance of S&C data-driven solutions (Melo et al., 2022).

Taking into account the availability of advanced computational resources for data processing, their visual analysis has emerged as a powerful tool for extracting useful insights and uncovering meaningful patterns that cannot be revealed by traditional techniques, enhancing tasks such as the estimation of critical variables, and operational process monitoring. In this sense, visual analytics is an efficient tool for analyzing massive and complex data to extract relevant information for effective process monitoring (Hu et al., 2018; Yousef et al., 2023). Nonetheless, challenges persist regarding the complexity of industrial sensor data (e.g., non-linearity, autocorrelation, and multimodality). It is crucial to improve the interpretability, visualization, and efficiency of S&C data-driven solutions while emphasizing the need to balance complexity in the machine learning techniques, and domain knowledge from process system engineering (Daoutidis et al., 2024; Yu and Zhang, 2023).

Data-driven process monitoring is a widely adopted solution in S&C (Ji and Sun, 2022; Qin et al., 2020; Ji et al., 2021; Chen and Jiang, 2022). It is often performed with principal components analysis (PCA) (Apsemidis et al., 2020; Nawaz et al., 2022). In general, data-driven process monitoring involves the application of statistical or machine learning methods to analyze sensor data and identify any pattern or trend indicating a potential abnormal operation that can cause serious damage to operators and/or equipment, increase downtime for maintenance, or quality reduction of final products (Qin et al., 2020). PCA is popular due to its dimensionality reduction capability and representing sensor data in the form of time-series data, by projecting it into a lower-dimensional feature space. Subsequently, a monitoring statistic variable, devoid of physical meaning, is calculated and then compared with a predefined threshold. However, sensor data could be collinear, necessitating a large amount of data, unusual conditions are misclassified as failures, or results are poorly interpreted (Ji and Sun, 2022). Visual analytics appears as a good alternative to PCA-based process monitoring because it transforms sensor data into visual representations, thereby converting process monitoring into image classification, and simultaneously enabling human supervision (Yousef et al., 2023).

Recent studies highlight the potential of visualization as a tool to assist decision-makers in comprehending data and identifying patterns (Ltifi et al., 2020). Additionally, intuitive graphical tools are designed for classifying smart factory operations (Wu et al., 2018), and time-series images are interpreted and analyzed using computer-vision techniques (Yousef et al., 2023). Advanced visualization plots were utilized to compare operating conditions using binary alarm data and sensor data (Hu et al., 2018). However, these methods often require a substantial amount of unlabeled, representative process information in terms of volume and variability, with non-trivial patterns.

The main contribution of this work is to examine the suitability of unsupervised machine learning (ML) methods for image analysis within an innovative visual analytics framework. This is done by developing a set of performance metrics that evaluate the reconstruction image capability and information content of the image analysis stage for visual analytics. These metrics are used to assess the performance of unsupervised ML methods in an operational regime, emphasizing the interpretability of the results. The operational regime in which the work is being performed is a real-world setting where the ML methods are used to analyze images in real-time.

The remainder of the paper is organized as follows. Section 2 presents some relevant preliminary concepts. The detailed methodology for visual analytics for process monitoring is presented in Section 3. The effectiveness of the proposed method is demonstrated using a case study in Section 4, followed by concluding remarks in Section 5.

2. BACKGROUND

For better understanding, relevant preliminary concepts are presented in this section. First, a brief description of time-series imaging is provided, followed by a discussion on the unsupervised ML methods for images and their performance metrics.

2.1 Time-series imaging

Time-series imaging involves converting a series of process variable measurements collected over time (1D data) into a visual representation suitable for analysis by ML methods (Yousef et al., 2023). This process provides information for any time-series $(x_1, x_2, \ldots, x_n)$, retaining the relationship between the original time-series and its visually transformed representation (Wang and Oates, 2015). These methods rely on encoding mappings with a unique inverse function, ensuring the preservation of temporal dependency. Various encoding frameworks, such as Gramian Angular Field, and Markov Transition Field, enable the visualization of time-series-based images by capturing temporal correlations, transition probabilities, and distances between trajectories, respectively (Wang and Oates, 2015; Jiang et al., 2022).

Gramian Angular Field (GAF): The fundamental principle of GAF involves representing a time-series, denoted as X, as a quasi-Gram Matrix, $\mathbf{G}$, where each element corresponds to the trigonometric sum between different time intervals (x_i, x_j) (Wang and Oates, 2015). To calculate

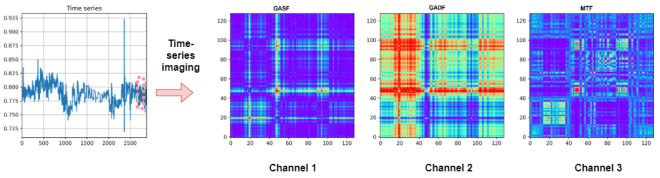

Fig. 1. An example of the time-series imaging of boiler energy efficiency for a rolling time window of 128 minutes.

either the Gramian Angular Summation Field (GASF) or the Gramian Angular Difference Field (GADF), the re-scaled time-series X^* (normalized to the interval $[-1, 1]$) is transformed into the polar coordinates. Subsequently, GAF leverages the angular perspective by calculating the trigonometric sum or difference between each point in X to identify the temporal correlation within distinct time intervals (x_i, x_j). GASF and GADF are defined as follows (Wang and Oates, 2015):

$$\begin{aligned} GASF(x_i, x_j) &= \cos(\theta_i + \theta_j); \\ GADF(x_i, x_j) &= \sin(\theta_i - \theta_j), \end{aligned} \tag{1}$$

where $\theta_i = \arccos(x_i^*)$ is the arc-cosine function over normalized vector X^*.

Markov Transition Field (MTF): Markov Transition Field (MTF) encodes dynamical transition statistics, based on Q quantiles. Thus, a $Q \times Q$ weighted adjacency matrix (MTF) is obtained by counting transitions among quantile bins in the manner of a first-order Markov chain along the time axis, as follows (Wang and Oates, 2015):

$$\text{MTF}(i, j) = w_{i,j} | x_i \in q_i, x_j \in q_j \tag{2}$$

The quantile bins that contain the data at time stamp i and j (temporal axes) are q_i and q_j ($q \in [1, Q]$). MTF(i, j) in the MTF denotes the transition probability of $q_i \rightarrow q_j$.

Fig. 1 illustrates a representative outcome (referential results) of time-series imaging for a rolling time window of 128 minutes; computing each image channel using GASF, GADF, and MTF methods. These results showcase noticeable color variations for each channel which represent a different method of time-series imaging.

2.2 Unsupervised ML methods for image analysis

We discuss two commonly used unsupervised ML methods for images dimensionality reduction, namely, autoencoders (AEs) and principal component analysis (PCA).

Principal Component Analysis: PCA is one of the most widely adopted methods for feature extraction in time-series data. By reducing the dimensionality of the original data space, PCA effectively preserves relationships among original variables through a set of latent variables in a feature space. This preservation of information is achieved through an eigenvector decomposition of either the covariance matrix or correlation matrix corresponding to a given dataset (Quiñones-Grueiro et al., 2019). Mathematically, PCA involves the eigenvector decomposition of the covariance matrix or correlation matrix for a given dataset $\mathbf{D}$ (size $n \times p$, where n is the number of observations and p is

the number of variables). PCA transforms $\mathbf{D}$ into a set of uncorrelated variables, namely, the principal components, represented by $\mathbf{Z}$. This transformation is given by,

$$\mathbf{D} = \mathbf{Z} \cdot \mathbf{P}^T + \mathbf{E}, \tag{3}$$

where $\mathbf{P}^T$ is the transpose of the eigenvector matrix (loadings) and $\mathbf{E}$ is the residual matrix of uncorrelated noise, which captures the information not accounted for by the retained principal components. Nonetheless, PCA is limited by the linear correlation structure of the variables in the feature space.

Auto-encoders: AEs are a type of unsupervised ML structures to encode input data into a lower-dimensional representation and subsequently decode it to the original input. They are particularly useful in handling high-dimensional data, like images. AEs serve various purposes, including dimensionality reduction, feature learning, denoising, data compression, and anomaly detection (Jaiswal et al., 2023; Li et al., 2023). AEs could be defined as follows:

$$\begin{aligned} h_i &= g(W_i), \\ \hat{W}_i &= f(h_i), \end{aligned} \tag{4}$$

where $g : \mathbb{R}^{L_1 \times L_2} \rightarrow \mathbb{R}^q$ is the encoder function to project the input image W_i of dimensions $L_1 \times L_2$ into a lower-dimensional feature space of dimension q. h_i represents the projection of image W_i in the features space, and $f : \mathbb{R}^q \rightarrow \mathbb{R}^{L_1 \times L_2}$ is the decoder function reconstructing an estimated image $\hat{W}_i$, expecting $\hat{W}_i \approx W_i$. Equation 4 represents the structure of the autoencoder, utilizing a feedforward neural network for encoding and decoding, commonly referred to as a vanilla autoencoder. An additional variant, the convolution autoencoder, combines the local convolution connections with the autoencoder, introducing a reconstruction input for the convolution operation.

3. METHODOLOGY

This section presents the detailed methodology for the application of visual analytics in process monitoring.

3.1 Visual analytics for process monitoring of a steam boiler

Chemical processes often deal with many process variables and visualization of process data in 2D plots is a commonly adopted approach by process operators/engineers to detect patterns and anomalies. Commonly, data-driven process monitoring is performed by calculating Hotelling's T^2 statistic over the result of multivariable dimensionality reduction with PCA/PLS, where T^2 statistic is compared with a threshold value (Ji and Sun, 2022). Such an approach requires having a large amount of process data. However, these methods have limitations, including their linear internal estimation structures, reliance on large datasets with high sample sizes, computational cost, the need to select the optimal number of latent variables, and the lack of a clear physical interpretation of latent variables in the feature space.

Through time-series imaging methods, visual analytics offer pixel-based representations of data, providing valuable information and insights into process conditions. This approach allows for generating images from a single representative time-series variable, enabling the analysis of patterns and textures that are interpretable by both operators and artificial intelligence compared to time-series signals. Human operators can easily comprehend how different patterns in the images correspond to specific operational conditions, improving the interpretability of the model. Additionally, visual analytics produce 2D images that retain temporal dependencies from the original time-series data, making them suitable for subsequent analysis using computer vision tools. Therefore, such a framework is adopted in this work for the monitoring of steam boilers.

Fig. 2 illustrates the application of visual analytics in the process monitoring of a steam boiler using the time series data for energy efficiency in three stages, namely, visual representation of time-series, image analysis, and monitoring. First, the raw time-series data for relevant process variables are converted into images. Then, the images are analyzed to detect anomalies using unsupervised ML methods. Finally, the results of the analysis are utilized by human operators for process monitoring and fault diagnostics.

3.2 Performance metrics

The commonly adopted key performance metrics to quantify the effectiveness of image reconstruction methods in visual analytics are the Mean Squared Error (MSE), Mean Absolute Error (MAE), Structural Similarity Index (SSIM), and Peak Signal-to-Noise Ratio (PSNR). Abnormal variations in two or more key performance metrics indicate potential failure states in the steam boiler.

Mean Squared Error (MSE): It quantifies the average of the squared differences between corresponding pixels in the original image and the reconstructed image and is determined as:

$$\text{MSE} = \frac{1}{N} \sum_{i=1}^{N} (I_i - I_i')^2, \tag{5}$$

where I denotes the original image, I_i' is the image calculated by the reconstruction method, and N is the total number of pixels in the image.

Mean Absolute Error (MAE): This metric calculates the average of the absolute differences between corresponding pixels as follows:

$$\text{MAE} = \frac{1}{N} \sum_{i=1}^{N} |I_i - I_i'|. \tag{6}$$

Structural Similarity Index (SSIM): This metric measures the structural similarity between the original and the reconstructed image and is expressed as:

$$\text{SSIM}(I, I') = \frac{(2\mu_I \mu_{I'} + c_1)(2\sigma_{I,I'} + c_2)}{(\mu_I^2 + \mu_{I'}^2 + c_1)(\sigma_I^2 + \sigma_{I'}^2 + c_2)}, \tag{7}$$

where μ_I and $\mu_{I'}$ represent the mean intensities, σ_I^2 and $\sigma_{I'}^2$ are the standard deviations, and c_1 and c_2 are small constants introduced to avoid division by zero.

Peak Signal-to-Noise Ratio (PSNR): This metric quantifies the ratio of the peak possible signal power to the

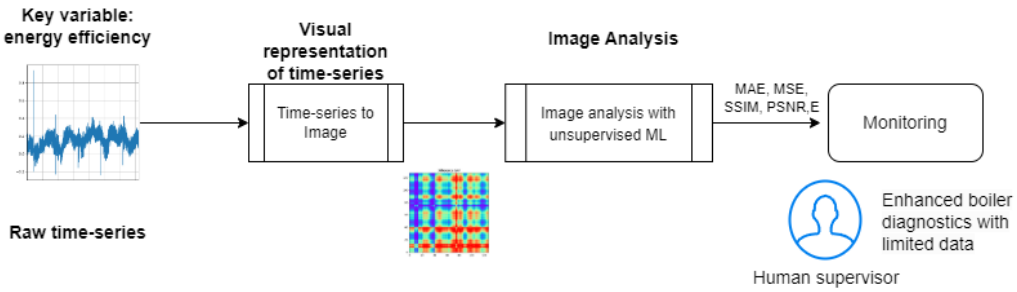

Fig. 2. Overview of the application of visual analytics for process monitoring and diagnostics.

power of the noise in the image. It is often expressed in decibels (dB) and is calculated as:

$$\mathrm{PSNR}(I, I') = 10 \cdot \log_{10}\left(\frac{R^2}{MSE}\right). \tag{8}$$

Here, R denotes the maximum pixel value (e.g., 255 for 8-bit images) and MSE is the Mean Squared Error in (5).

Shannon Entropy: This metric, represented by E, is a measure of the information content within a given source, particularly an image (Liu et al., 2015). Consequently, when evaluating a time-series imaging task, maximizing entropy is desirable. This maximization ensures the maximum amount of information is passed on to the image analysis stage in the visual analytics path. In this work, the Shannon entropy (of a single-channel) I_l is calculated as (Wu et al., 2013):

$$E(I_l) = -\sum_{k=1}^{L} p(x_k) \cdot \log_2(p(x_k)), \tag{9}$$

where L is the number of possible intensity levels in the image; x_k represents each possible intensity level in the image; $p(x_k)$ gives the probability of occurrence of the intensity level x_k in the image (obtained from the normalized image histogram). In the case of images with an arbitrary number of channels, denoted by N_{ch}, (here, $N_{ch} = 3$), the entropy is determined as the average value, denoted by, $\bar{E}(I_l)$, for each channel as:

$$\bar{E}(I_l) = \frac{1}{N_{ch}} \sum_{k=1}^{N_{ch}} E(I_l). \tag{10}$$

These metrics provide diverse insights into the quality of the reconstructed images. Lower MSE and MAE values indicate superior reconstruction, while higher SSIM and PSNR values suggest higher image fidelity. Additionally, anomalous behavior in the process is indicated by unusual variability of these computed performance indices, including MSE, MAE, SSIM, PSNR, and Entropy. Next, the above-mentioned unsupervised ML methods are utilized in the process monitoring based on image analysis. Also, the entropy of the image is used to assess the quality of the feature extraction.

4. CASE STUDY

The applicability and effectiveness of the proposed visual analytics framework are demonstrated through a case study using data from a real industrial steam boiler.

4.1 Process monitoring of boilers

The case studies are performed on a time-series dataset obtained from an industrial steam boiler. The data comprise 37440 measurements with a sampling period of $T_s = 1$ minute. To evaluate the performance of the proposed approach with distorted data, synthetic distortion was applied to the original time-series data for energy efficiency in the form of (1) additive Gaussian noise and (2) a constant abnormal value of -1. Time series imaging methods are then applied in a rolling time window of 60 minutes on the energy efficiency time-series. This creates a GASF, GADF, and MTF matrices of dimension 32×32 for each time window, resulting in an image channel per each imaging method.

In a steam boiler, process variables are related to factors, such as fuel and airflow, water level within the dome, internal pressure, outlet steam temperature, pressure, and mass flow. However, the most critical variable for process monitoring of boiler operation is the energy efficiency of the boiler. It is determined as the ratio between the energy output in steam and the energy input from fuel and blended gas flow, as follows (Baukal Jr, 2010):

$$\eta(k) = \frac{q(k)}{m_{oil}(k) \cdot \mathrm{HHV}_{oil} + f_{gm}(k) \cdot \mathrm{HHV}_{gm} \cdot d_{gm}}, \tag{11}$$

where $q(k)$ is the heat transfer rate to the steam, which depends on the steam mass flow m_s and steam enthalpy; HHV_{oil} and HHV_{gm} are the high heating value of oil and blend gas fuels, respectively, while d_{gm} stands for the blended gas density. Please note that the values of HHV_{gm} and d_{gm} are obtained from laboratory analysis. Steam enthalpy is calculated as a function of the steam pressure p_s and temperature T_s. Results of the exploratory data analysis are provided in Table 1, where it is observed that maximum values are reached in the training dataset.

4.2 Results of process monitoring by visual analytics

Unsupervised machine learning methods, namely, PCA and AE (vanilla and convolutional), were employed for image projection into feature space and subsequent visual analytics. Both methods were evaluated using the performance metrics discussed in Section 3.2.

For PCA, the optimal number of components or latent variables was determined offline with a threshold of 95% of total information retained, giving a result of 222 components. The image entropy was calculated to quantify the information derived from the time-series imaging process. Please note that the abnormal behavior in the process would be detected by an abnormal variability in the calculated performance indices.

Now, the results from the visual analytics framework are presented. Firstly, Fig. 3 illustrates the visual analytics results of the performance indices for unsupervised learning methods (Convolutional AE, Vanilla AE, and PCA), from the original energy efficiency time-series data from the boiler. Last row of Fig. 3 shows the Hotelling's T^2 statistics and its threshold value, as a benchmark result of process monitoring based on multivariate analysis with PCA and the full information from the process through sensors data. Secondly, Figs. 4 and 5 present the visual analytics result, now incorporating the synthetic distortion of additive Gaussian noise in the testing data with different values of variance: high and low, and large distance between distorted measurements. Additive Gaussian noise in the energy efficiency time-series could be related to a distortion in the communications channel or the sensor's physical connection. Finally, Fig. 6 shows the visual analytics results with missing values, that are considered constant values in the original boiler energy efficiency time-series. Missing values in the boiler energy efficiency time-series are related to a constant abnormal value without physical significance (in this case, the abnormal value is -1). In these figures, light blue, light green, and orange windows represent training, validation, and testing data, respectively.

4.3 Discussion

The results from visual analytics of the steam boiler are discussed, providing some process knowledge to explain the behavior. From Fig. 3, it is observed that MSE and MAE increase with a sudden change in the test dataset for all unsupervised methods. This sudden change is also evident in the performance indices, namely, SSIM, PSNR, and entropy, possibly explained by an abnormal calculation of the energy transferred to the steam, which distorts energy efficiency calculation. According to the normal variations in the steam pressure, temperature and combustion, the normal variations in energy efficiency are slow and smoothed. PCA exhibits improved accuracy in image reconstruction with small MSE and MAE, showcasing its strong generalization capabilities. However, caution must be exercised when detecting small variations and the number of principal components chosen. Hotelling's T^2 statistics indicate that the threshold for abnormal steam boiler behavior is being surpassed, suggesting that there may be false positive detections of anomalies.

Table 1. Summary statistics for the steam boiler energy efficiency

Set	N	Mean	Std	Min	25%	50%	75%	Max
Train	18,720	0.741	0.069	0.565	0.686	0.750	0.795	0.942
Validation	9,360	0.676	0.093	0.532	0.556	0.709	0.746	0.846
Test	9,360	0.589	0.046	0.519	0.574	0.586	0.600	0.828

In the cases of synthetic distortion by additive Gaussian noise in the energy efficiency (Figs. 4 and 5), a high abnormal value of MSE and MAE is observed, accompanied by decreased values of SSIM and PSNR. This behavior can be explained by the corruption of the normal time-series captured by visual analytics with AE. Convolutional AE is more sensitive to the Gaussian noise since exhibits a slightly high value of MAE and MSE during the distortion, compared to vanilla AE. Conversely, PCA is less affected, where high noise did not distort MSE and MAE. Additionally, SSIM and PSNR exhibit non-drastic variations with PCA. Note that, entropy remained unaffected by the synthetic additive Gaussian noise with AEs.

For the synthetic distortion of the constant abnormal value of -1 related to missing data, results in Fig. 6 show that performance indices, namely, MAE and MSE remain constant with sudden peak values highlighting the abnormal behavior in the original time-series. Besides, SSIM and PSNR decreases for both AE and PCA. Regarding entropy, as shown in Fig. 6, distorted behavior is observed because a constant value remains in an image without variability, resulting in null entropy.

In summary, autoencoders (AE) in the visual analytics framework prove capable of learning the expected behavior of energy efficiency of the boiler, demonstrating its applicability in the process monitoring of boilers. The abnormal energy efficiency values are revealed as abnormal values of the performance indices (MSE, MAE, SSIM, PSNR, or entropy), mainly with visual analytics considering AE.

5. CONCLUSIONS

This study examined the applicability and effectiveness of unsupervised machine learning methods, namely, principal component analysis (PCA) and autoencoders (AEs), in process monitoring through visual analytics. Promising results from an industrial case study demonstrate the capability of visual analytics to detect abnormal variations in the energy efficiency dataset of an industrial steam boiler. The implementation of unsupervised training in an autoencoder designed for boiler diagnostics enables this detection, utilizing a limited dataset. As an exploratory work, future research may delve into a comprehensive evaluation of process monitoring methods and visual analytics employing more complex ML structures for fault detection in industrial processes, including transformers.

ACKNOWLEDGEMENTS

Hugo O. Garcés is grateful for the support from ANID (Chile), through grant FONDECYT Regular No 1220903.

REFERENCES

Annaswamy, A.M., Johansson, K.H., and Pappas, G.J.E. (eds.) (2023). *Control for societal-scale challenges: Road map 2030.* IEEE Control Systems Society.

Apsemidis, A., Psarakis, S., and Moguerza, J.M. (2020). A review of machine learning kernel methods in statistical process monitoring. *Computers & Industrial Engineering*, 142, 106376.

Baukal Jr, C.E. (2010). *Industrial Combustion Testing.* Taylor and Francis.

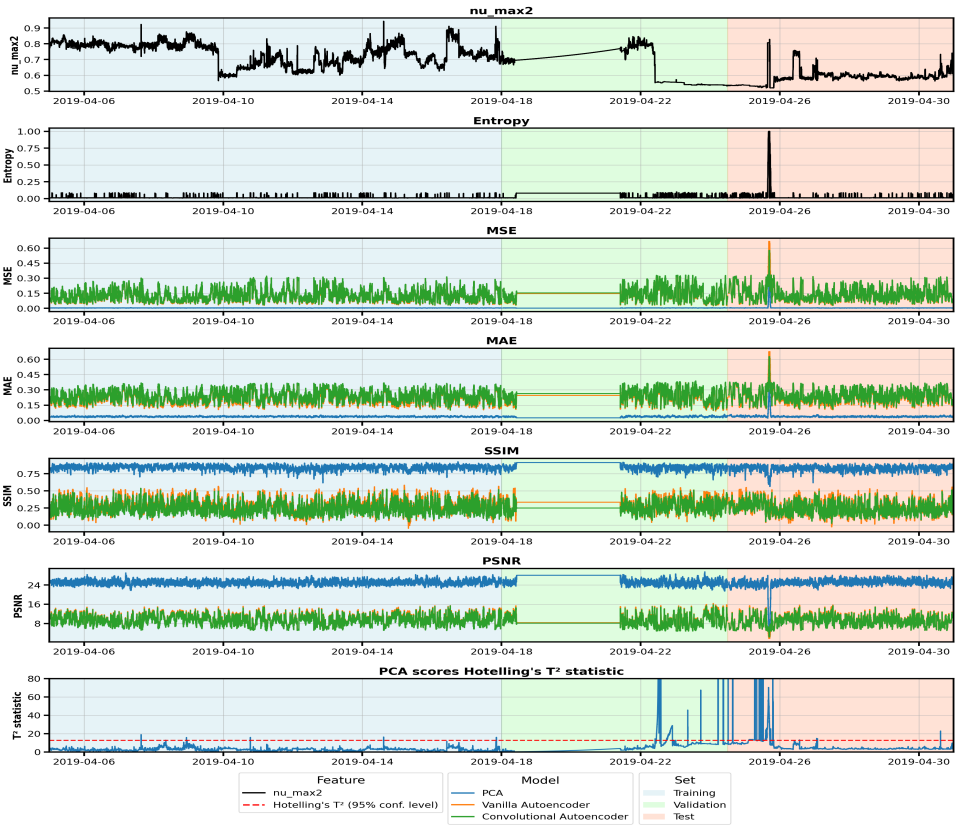

Fig. 3. Performance indices for boiler diagnostics through visual analytics using the original energy efficiency time-series.

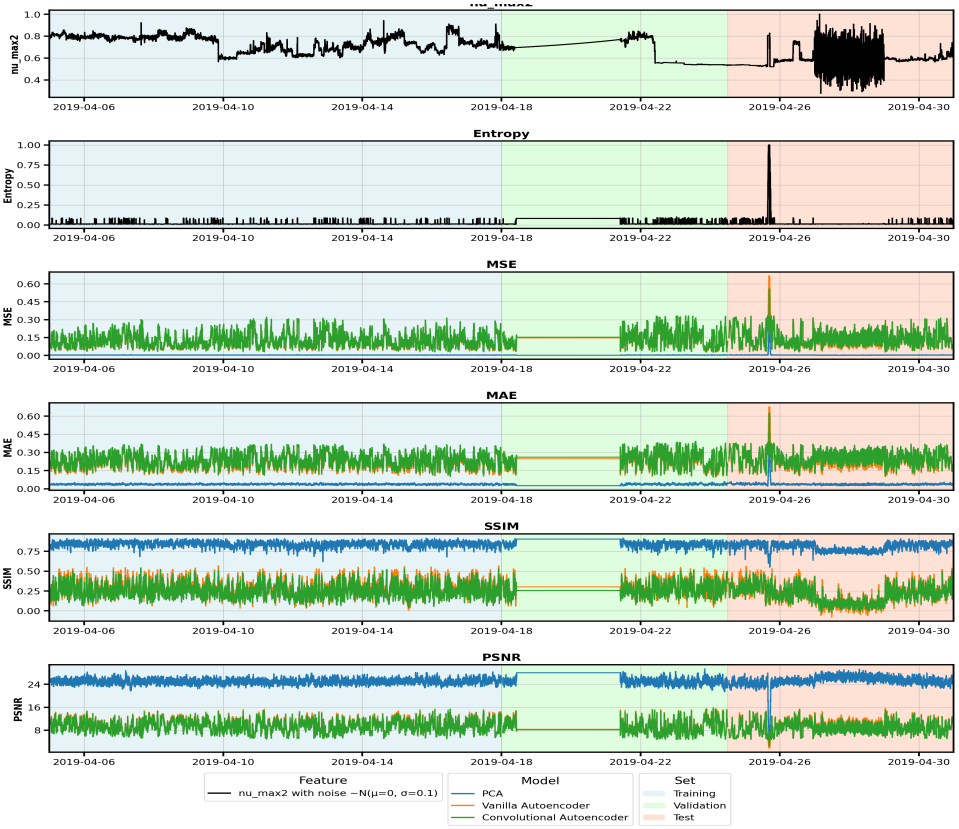

Fig. 4. Performance indices for boiler diagnostics through visual analytics using the energy efficiency time-series with "Gaussian noise" failure of high variance.

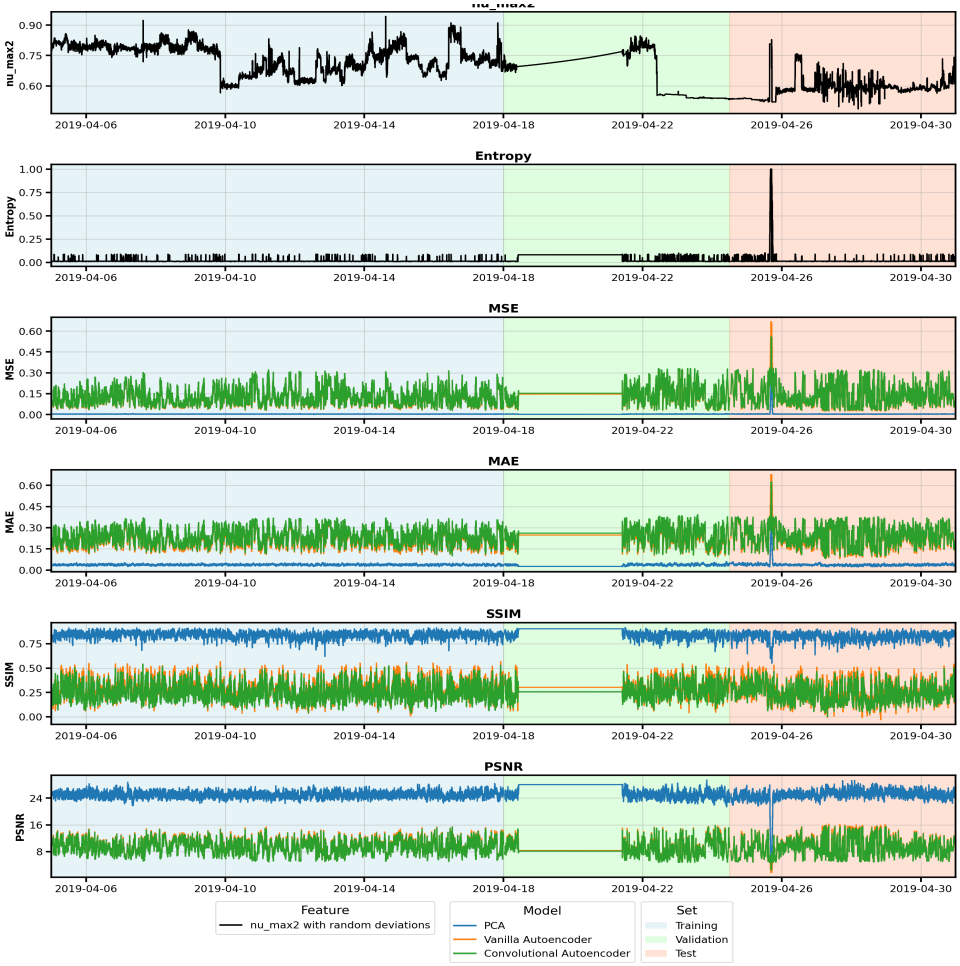

Fig. 5. Performance indices for boiler diagnostics through visual analytics using the energy efficiency time-series with "Gaussian noise" failure of low variance and large distance between distorted measurements.

Chen, S. and Jiang, Q. (2022). Distributed Robust Process Monitoring Based on Optimized Denoising Autoencoder With Reinforcement Learning. *IEEE Transactions on Instrumentation and Measurement*, 71, 1–11.

Daoutidis, P., Lee, J.H., Rangarajan, S., Chiang, L., Gopaluni, B., Schweidtmann, A.M., Harjunkoski, I., Mercangöz, M., Mesbah, A., Boukouvala, F., Lima, F.V., del Rio Chanona, A., and Georgakis, C. (2024). Machine learning in process systems engineering: Challenges and opportunities. *Computers & Chemical Engineering*, 181, 108523.

Hu, W., Al-Dabbagh, A.W., Chen, T., and Shah, S.L. (2018). Design of visualization plots of industrial alarm and event data for enhanced alarm management. *Control Engineering Practice*, 79, 50–64.

Jaiswal, G., Rani, R., Mangotra, H., and Sharma, A. (2023). Integration of hyperspectral imaging and autoencoders: Benefits, applications, hyperparameter tunning and challenges. *Computer Science Review*, 50, 100584.

Ji, C. and Sun, W. (2022). A Review on Data-Driven Process Monitoring Methods: Characterization and Mining of Industrial Data. *Processes*, 10(2), 335. Number: 2 Publisher: Multidisciplinary Digital Publishing Institute.

Ji, C., Wang, J., and Sun, W. (2021). A nonstationary process monitoring based on mutual information among process variables. *IFAC-PapersOnLine*, 54(3), 451–456.

Jiang, W., Zhang, D., Ling, L., and Lin, R. (2022). Time series classification based on image transformation using feature fusion strategy. *Neural Processing Letters*, 54(5), 3727–3748.

Lawrence, N.P., Damarla, S.K., Kim, J.W., Tulsyan, A., Amjad, F., Wang, K., Chachuat, B., Lee, J.M., Huang, B., and Bhushan Gopaluni, R. (2024). Machine learning for industrial sensing and control: A survey and practical perspective. *Control Engineering Practice*, 145, 105841.

Li, P., Pei, Y., and Li, J. (2023). A comprehensive survey on design and application of autoencoder in deep learning. *Applied Soft Computing*, 138, 110176.

Liu, X.Y., Li, R.L., Zhao, H.W., Cheng, T.H., Cui, G.J., Tan, Q.C., and Meng, G.W. (2015). Quality assessment of speckle patterns for digital image correlation by shannon entropy. *Optik*, 126(23), 4206–4211.

Ltifi, H., Kolski, C., and Ben Ayed, M. (2020). Survey on Visualization and Visual Analytics pipeline-based models: Conceptual aspects, comparative studies and challenges. *Computer Science Review*, 36, 100245.

Melo, A., Câmara, M.M., Clavijo, N., and Pinto, J.C. (2022). Open benchmarks for assessment of process monitoring and fault diagnosis techniques: A review and

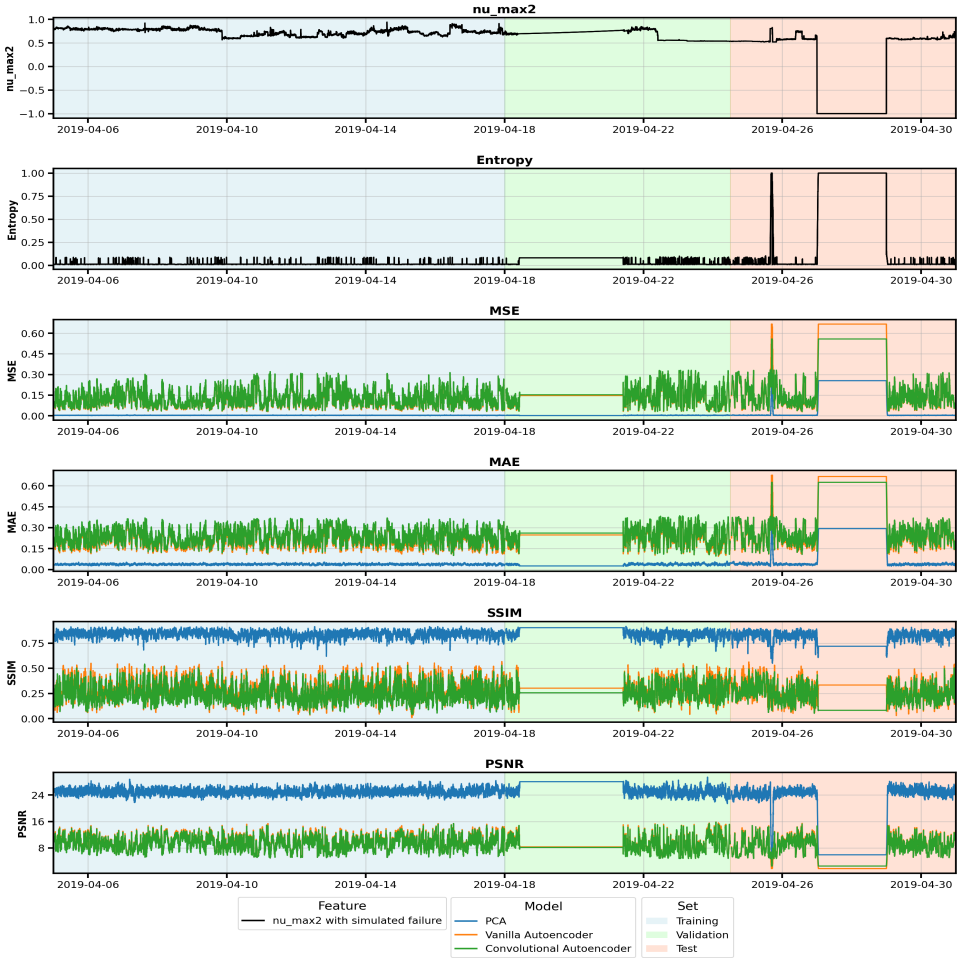

Fig. 6. Performance indices for boiler diagnostics through visual analytics using the energy efficiency time-series with synthetic "missing value" failure.

critical analysis. *Computers & Chemical Engineering*, 165, 107964.

Nawaz, M., Maulud, A.S., Zabiri, H., and Suleman, H. (2022). Review of Multiscale Methods for Process Monitoring, With an Emphasis on Applications in Chemical Process Systems. *IEEE Access*, 10, 49708–49724.

Qin, S.J., Dong, Y., Zhu, Q., Wang, J., and Liu, Q. (2020). Bridging systems theory and data science: A unifying review of dynamic latent variable analytics and process monitoring. *Annual Reviews in Control*, 50, 29–48.

Quiñones-Grueiro, M., Prieto-Moreno, A., Verde, C., and Llanes-Santiago, O. (2019). Data-driven monitoring of multimode continuous processes: A review. *Chemometrics and Intelligent Laboratory Systems*, 189, 56–71.

Wang, Z. and Oates, T. (2015). Imaging time-series to improve classification and imputation. In *Proceedings of the 24th International Joint Conference on Artificial Intelligence (IJCAI 2015)*, 3939–3945.

Wu, W., Zheng, Y., Chen, K., Wang, X., and Cao, N. (2018). A Visual Analytics Approach for Equipment Condition Monitoring in Smart Factories of Process Industry. In *2018 IEEE Pacific Visualization Symposium (PacificVis)*, 140–149. IEEE, Kobe.

Wu, Y., Zhou, Y., Saveriades, G., Agaian, S., Noonan, J.P., and Natarajan, P. (2013). Local Shannon entropy measure with statistical tests for image randomness. *Information Sciences*, 222, 323–342.

Yousef, I., Tulsyan, A., Shah, S.L., and Gopaluni, R.B. (2023). Visual analytics for process monitoring: Leveraging time-series imaging for enhanced interpretability. *Journal of Process Control*, 132, 103127.

Yu, J. and Zhang, Y. (2023). Challenges and opportunities of deep learning-based process fault detection and diagnosis: a review. *Neural Computing and Applications*, 35(1), 211–252.